Keck Spectroscopy of Redshift $z \sim 3$ Galaxies in the Hubble Deep Field [1]

James D. Lowenthal[2], David C. Koo, Rafael Guzmán, Jesús Gallego

Andrew C. Phillips, S. M. Faber, Nicole P. Vogt, Garth D. Illingworth

and

Caryl Gronwall

UCO/Lick Observatory and Board of Astronomy and Astrophysics, University of California, Santa Cruz, CA 95064.
email: james, koo, rguzman, jgm, phillips, faber, nicole, gdi, caryl@ucolick.org

ABSTRACT

We have obtained spectra with the 10-m Keck telescope of a sample of 24 galaxies having colors consistent with star-forming galaxies at redshifts $2 \lesssim z \lesssim 4.5$ in the Hubble Deep Field (HDF). Eleven of these galaxies are confirmed to be at high redshift ($z_{\mathrm{med}} = 3.0$), one is at $z = 0.5$, and the other 12 have uncertain redshifts but have spectra consistent with their being at $z > 2$. The spectra of the confirmed high-redshift galaxies show a diversity of features, including weak Lyα emission, strong Lyα breaks or damped Lyα absorption profiles, and the stellar and interstellar rest-UV absorption lines common to local starburst galaxies and high-redshift star-forming galaxies reported recently by others. The narrow profiles and low equivalent widths of C IV, Si IV, and N V absorption lines may imply low stellar metallicities. Combined with the 5 high-redshift galaxies in the HDF previously confirmed with Keck spectra by Steidel *et al.* (1996b), the 16 confirmed sources yield a comoving volume density of $n \geq 2.5 \times 10^{-4}~h_{50}^3~\mathrm{Mpc}^{-3}$ for $q_0 = 0.05$, or $n \geq 1.2 \times 10^{-3}~h_{50}^3~\mathrm{Mpc}^{-3}$ for $q_0 = 0.5$. These densities are $3 - 4$ times higher than the recent estimates of

---

[2]Hubble Fellow

arXiv:astro-ph/9612239v1 30 Dec 1996

Steidel *et al.* (1996a) based on ground-based photometry with slightly brighter limits, and are comparable to estimates of the local volume density of galaxies brighter than L*. The high-redshift density measurement is only a lower limit, and could be almost three times higher still if all 29 of the unconfirmed candidates in our original sample, including those not observed, are indeed also at high redshift. The galaxies are small but luminous, with half-light radii $1.8 < r_{1/2} < 6.5$ h_{50}^{-1} kpc and absolute magnitudes $-21.5 > M_B > -23$. The HST images show a wide range of morphologies, including several with very close, small knots of emission embedded in wispy extended structures. Using rest-frame UV continuum fluxes with no dust correction, we calculate star formation rates in the range $7 - 24$ or $3 - 9$ h_{50}^{-2} M$_\odot$ yr^{-1} for $q_0 = 0.05$ and $q_0 = 0.5$, respectively. These rates overlap those for local spiral and H II galaxies today, although they could be more than twice as high if dust extinction in the UV is significant. If the objects at $z = 3$ were simply to fade by 5 magnitudes (assuming a 10^7 yr burst and passive evolution) without mergers in the 14 Gyr between then and now (for $q_0 = 0.05, h_{50} = 1.0$), they would resemble average dwarf elliptical/spheroidal galaxies in both luminosity and size. However, the variety of morphologies and the high number density of $z = 3$ galaxies in the HDF suggest that they represent a range of physical processes and stages of galaxy formation and evolution, rather than any one class of object, such as massive ellipticals. A key issue remains the measurement of masses. These high-redshift objects are likely to be the low-mass, starbursting building blocks of more massive galaxies seen today.

Subject headings: Galaxies: Redshifts – Galaxies: Evolution – Galaxies: Formation – Galaxies: Starburst – Cosmology

1. Introduction

Finding and studying populations of high-redshift galaxies is one of the major goals of contemporary observational cosmology (Bahcall 1991). By directly observing galaxies at lookback times corresponding to 90% of a Hubble time or more ($z \geq 3$ for $q_0 \geq 0.05$), we can empirically constrain models of the formation and evolution of galaxies.

It has been known for some time that broad-band colors can provide an excellent means of estimating galaxy redshifts (e.g. Koo 1985; Lilly, Cowie, & Gardner 1991; Connolly *et al.* 1995), but only recently, with the advent of 10-m class telescopes, have relatively normal

galaxies at $z > 2$ become accessible for spectroscopic confirmation. Because the spectra of cosmologically distant, actively star-forming galaxies show strong breaks at redshifted Lyα and the Lyman continuum — imposed by internal interstellar absorption, intervening HI clouds, the diffuse intergalactic medium, and other galaxies (*e.g.*, Madau 1995) — they can be recognized via their generally blue colors coupled with a dramatic dropoff in U or B ("*U*-" or "*B*-dropouts"), corresponding to the redshifted Lyα or Lyman continuum break passing through those bands.

Steidel *et al.* (1996a) have pioneered the technique of using deep broad-band photometry to isolate such Lyman-break galaxies, obtaining confirming spectra at the 10-m W. M. Keck Telescope and high-resolution images with the 2.4-m Hubble Space Telescope (*HST*) (Giavalisco *et al.* 1996). They found that this newly-discovered population of $z > 3$ galaxies exhibit stellar and interstellar absorption lines characteristic of local starburst galaxies, as well as occasional Lyα emission lines. The objects have small sizes ($1.5 < r_{1/2} < 3\ h_{50}^{-1}$ kpc), high luminosities $L > L^*$ and star formation rates 12 - 75 h_{50}^{-2} M$_\odot$ yr^{-1} (for $q_0 = 0.05$). For $R_{AB} < 25.0$ and redshifts 3.0 - 3.5, the volume density was found to be 0.1 - 0.5 times that of $L > L^*$ galaxies today.

The Hubble Deep Field (HDF; Williams *et al.* 1996) provides an unprecedented opportunity for locating and studying such high-redshift galaxies. With a total of 150 orbits of HST time invested in the F300W, F450W, F606W, and F814W WFPC2 filters, final sensitivities exceeded $I_{814,AB} = 28$ (3σ) in a single WFPC2 field with area 4.7 arcmin^2. The HDF includes well over 1000 galaxies down to those levels.

In this paper, we present spectra obtained at the Keck telescope of a sample of U- and B-dropout galaxies selected by color to have $z \sim 3$ in the HDF. This sample, observed as part of the "DEEP" program,[3] is similar to that observed by Steidel *et al.* (1996b) in the HDF. However, it has yielded more than twice the number of confirmed redshifts $z > 2.2$ and pushes roughly one magnitude deeper, sampling further down the luminosity function of distant star-forming galaxies, and significantly increasing the volume density of known high-redshift galaxies.

---

[3]Deep Extragalactic Evolutionary Probe; see http://www.ucolick.org/~deep/home.html for more information

2. The Sample

Many groups (*e.g.*, Koo 1985; Bruzual & Charlot 1993; Madau 1995; Gronwall & Koo 1995) have spent considerable effort studying the expected colors of high-redshift galaxies in detail, including through extensive modeling using synthetic and observed galaxy spectra, stellar population considerations, and radiative transfer effects, and more recently through analysis of deep spectroscopic surveys. For our observations of galaxies in the HDF, given the constraints of field size, observing time and the relative immaturity of the technique, we chose a simple set of selection criteria that maximized the chances of finding high-redshift galaxies, but were not fine-tuned to exclude interlopers.

We used the photometric catalog of objects in the HDF prepared by the HDF team using FOCAS on the Version 1 "drizzled"[4] dataset to select our sample. We examined the distributions of isophotal colors and magnitudes and selected 39 U-dropout objects, i.e. blue in "$B - I$" ($B_{450} - I_{814} < 1.22$)[5] but extremely red in "$U - B$" ($U_{300} - B_{450} > 1.41$), the colors expected for a blue, star-forming galaxy at $2 < z < 3.5$ with a Lyman continuum break (*e.g.*, Madau 1996). Objects selected were brighter than $(V_{606} + I_{814})/2 = 25.5$ to help guarantee adequate signal-to-noise ratios (SNRs) in the spectra. Allowing objects up to one magnitude fainter into the sample would have roughly doubled the number of candidates. (Note that many of the candidate objects do not completely disappear in the F300W image – the Lyman continuum break falls within the F300W filter for $1.2 < z < 2.6$ – although we retain the terminology "dropout.")

We also selected 11 B-dropout candidates. Such objects are blue in "$V - I$" ($V_{606} - I_{814} < 0.37$) but extremely red in "$B - V$" ($B_{450} - V_{606} > 0.85$), and also have $(V_{606} + I_{814})/2 < 25.5$. They result because (i) cosmologically intervening material is expected to cause not only a Lyman continuum break but also a significant Lyα break (up to 1 magnitude at $z = 4$; Madau 1995); and (ii) the Lyman continuum break passes into the F450W filter for $z > 3.4$. Four of these 11 B-dropout objects were already in the U-dropout sample; thus we had a total sample of 46 candidate high-redshift galaxies in the HDF. Five of these were observed by Steidel *et al.* (1996b), so we eliminated them from our target list (although we were able to observe object C4-09 in the same slitlet used

---

[4]The drizzled images result from a flux-conserving technique of combining individual WFPC2 images registered to sub-pixel accuracy. All four chips (WF and PC) are resampled to $0\rlap{.}''04$ pixels. See http://www.stsci.edu/ftp/observer/hdf for more information.

[5]Note that we are using AB magnitudes throughout, transformed from ST magnitudes as detailed in the HDF information posted on the World Wide Web: to transform from ST magnitudes to AB magnitudes, add 1.31, 0.399, -0.199, and -0.819 to U_{300}, B_{450}, V_{606}, and I_{814}, respectively.

for two other objects), leaving a final sample of 41 new candidates. We verified that our selection recovered all but one of Steidel *et al.*'s 18 additional candidates. Note that no morphological or size criterion of any sort was applied.

FOCAS splits large, complex "parent" objects into smaller "offspring"; for our candidates, both parent and offspring objects often satisfied the selection criteria. We chose almost exclusively the parent object, which was generally brighter and larger than its offspring. We inspected the image of each candidate visually to verify that this assignment matched the appearance (spatial location and apparent magnitude) of the candidate without including other objects that were obviously unrelated, *e.g.*, bright stars.

In Fig. 1 we show a mosaic of the 25 objects that we observed (except for one object – hd2_1918_1912, which turned out to be a Galactic star also observed by Steidel *et al.* 1996b), excised in $10'' \times 10''$ boxes from the F814W HDF images. The sample exhibits a wide variety of morphologies. While it can be immediately seen from Fig. 1 that almost all the targets are small – with most of the light contained in $3''$ and usually within $1''$ – only a relatively small fraction (6 of 24, or 25%) have simple, symmetrical, isolated profiles. The remaining three-quarters all exhibit various degrees of sub-clumping; extremely close companions with colors similar enough to imply physical connection; extended, wispy structures; or combinations thereof. (Note, however, that we see at most one example – hd2_1739_1258 – of a "chain galaxy" similar to those reported by Cowie, Hu, & Songaila 1995).

3. Observations

We used the Low Resolution Imaging Spectrograph (LRIS; Oke *et al.* 1995) on the 10-m Keck telescope to obtain spectra on the nights of 22-24 April 1996 UT. Five multi-object slit masks typically covered 10 high-redshift candidates at a time in the HDF, plus another 20 objects in the "flanking fields" selected for different programs (Guzmán *et al.* 1996; Phillips *et al.* 1996; Vogt *et al.* 1996). Most of the high-redshift candidates were observed with more than one mask. Each slitlet was $1''.1$ wide and at least $10''$ long. The slits were up to $20''$ long in those cases when multiple objects could be covered by a single slit, which was then tilted to the appropriate position angle. We took care beforehand to derive accurate astrometric solutions for the HDF and the flanking fields (see our page on the World Wide Web for details), and saw no evidence in the data for astrometric errors. The seeing ranged from $0''.7$ to $1''.1$ FWHM with photometric conditions prevailing on all three nights.

We chose to use two moderate-resolution gratings — both 600 l/mm and blazed at 5000 Å (blue) and 7500 Å (red) — rather than one low-resolution grating. This

choice helped in subtraction of bright night sky emission lines and provided the best information possible on emission and absorption line widths and profiles. The slit and grating combinations produced a spectral resolution of 4.5 Å FWHM at 5500 Å, or about 240 km s^{-1} ($\sigma = 100$ km s^{-1}), for a source that completely fills the slit. However, for the objects discussed here, which are almost all unresolved at ground-based seeing, the resolution is determined by the seeing disk and not the slit. In this case, the resolution is ~ 3.4 Å FWHM, or $\sigma = 185$ km s^{-1}. The spectral coverage was complete from about 4000 Å to 9000 Å, the exact range depending on the location of the individual slitlets on the slit masks. Exposure times were 2×1500 sec per mask in each of the two gratings, for a total of 6,000 sec (8 targets, observed with only one mask) or 12,000 sec (17 targets, observed with two masks) per object, evenly split between the two gratings..

The data were reduced and analyzed using IRAF tasks and some of our own custom software. The images were bias-subtracted, flat-fielded, cosmic-ray cleaned, rectified using an analytical model to remove geometrical optical distortion and to straighten the spectra obtained through tilted slits, and sky-subtracted. Finally the two-dimensional images were co-added for each individual object and optimally extracted to a one-dimensional format. In practice, only the blue spectra were useful, as the blue colors of our sample galaxies meant that the continuum was often not visible in the red. Wavelength calibration was performed on the rebinned, two-dimensional spectra by using the bright 5577 Å O I night sky emission line as a zero-point reference; rms errors in the solutions are < 0.2 Å.

Table 1 lists the name, coordinates, apparent magnitude, color, class (U- or B-dropout), and exposure time of all 25 objects. In those cases for which the FOCAS catalog gave $U_{300,AB} > 28.0$, close to the detection limit for a compact ($< 1''$) source in the HDF, we list a conservative lower limit to $U - B$ calculated for $U_{300,AB} = 28.0$. In theory, the catalog contains useful information on the SNR of each object that could be applied on a case-by-case basis. However, at the time of our sample selection the noise properties of the HDF were not well characterized, so we chose the simpler and more robust route. In a few cases, measurement errors at these faint magnitudes meant that only the parent object met the color selection criteria and not the offspring, or vice versa; in these cases the candidate was retained although the tabulated color might lie slightly outside the selection zone.

4. Redshifts and Spectral Characteristics

We show in Fig. 2 one- and two-dimensional spectra for the 12 objects that yielded secure redshifts. Six of these exhibit single emission lines that we identify as Lyα; almost all show either a significant Lyα break or a damped Lyα absorption profile. In addition,

many of the spectra show the strong stellar and interstellar absorption lines of O I, Si II, C II, Al II, and C IV that are seen in other recently-reported high-redshift galaxies (Steidel *et al.* 1996a; Ebbels *et al.* 1996; Yee *et al.* 1996; Trager *et al.* 1996); in some cases, these features are the only ones that indicate the redshift. Only one object, hd4_1229_1791, was found to be at $z < 2$. Table 2 lists all twelve of the confirmed redshifts.

In an attempt to extract redshifts from those spectra with low SNR, we cross-correlated each spectrum with a one-dimensional spectrum of NGC 1741, a nearby starburst/Wolf-Rayet (WR) galaxy, obtained by Conti, Leitherer, & Vacca (1996) with HST and the Goddard High Resolution Spectrograph and kindly provided in digital form by C. Leitherer. In every case where there were obvious spectral features, the cross-correlation function showed a strong and isolated peak. However, in those cases without strong spectral features, the cross-correlation generally produced unconvincing results that we took only as a suggestion to be followed up with a visual search for identifiable spectral features. These uncertain values are shown in column 2 of Table 3.

There are at least two objects that show evidence for multiple absorption systems at different redshifts. One of these, hd4_1076_1847, is the brightest galaxy in the sample but has not yet yielded a confirmed redshift. This object is located in an especially complex region, only $3''$ from object C4-09 at $z = 3.22$ (Steidel *et al.* 1996b), $7''$ from hd4_1229_1791 at $z = 0.483$ (the only confirmed redshift $z < 1$ in our study), $2''$ north of a galaxy at $z = 1.010$ observed by Cohen *et al.* (1996), and $1''.5$ east of a galaxy at $z = 0.882$, also observed by Cohen *et al.*. These latter two objects are apparently responsible for Mg II $\lambda\lambda$ 2796, 2803 absorption visible at those redshifts in our spectrum, which is shown in Fig. 3. The projected distance of $1.5''$- $2''$ between hd4_1076_1847 and the absorbing galaxies corresponds to 15 - 20 h_{50}^{-1} kpc ($q_0 = 0.05$) at $z \sim 1$, well within the range of typical absorption cross-sections for QSO Mg II absorption line clouds (Drinkwater, Webster, & Thomas 1993; Steidel 1995). Galaxy hd4_1076_1847 may itself be at $z = 1.01$, of course, although we tentatively assign $z = 2.15$ based on possible C IV λ1550 (and maybe Al II) absorption.

The other object showing evidence for multiple redshift absorption is hd2_0698_1297, which has its own confirmed redshift of $z = 3.430$. We find weak absorption lines plausibly matching Si II 1260 Å and O I 1303 Å at $z = 3.368$, the redshift of hd2_0705_1366, only $3''$, or 12 h_{50}^{-1} kpc projected distance ($q_0 = 0.05$), away (although the signal-to-noise ratio is low). This is again comparable to typical absorption cross-sections of Mg II-selected galaxies at moderate redshifts.

Tables 2 and 3 give the redshift obtained for every object in the sample. The redshift quality Q_z is given on a scale from 1 to 4 such that $Q_z = 1$ means there is little hope of

assigning a redshift given the SNR in our data, 2 means real features are evident but the redshift is not secure, 3 means the redshift is probable, and $Q_z = 4$ means the redshift is definitely secure, with multiple spectral features identified.

The median redshift for the 11 galaxies in our sample with $Q_z \geq 3$ and $z > 2$ ("confirmed high redshift") is $z_{\mathrm{med}} = 3.0$; restricting the sample to $Q_z = 4$ does not change the median. Eight of the confirmed high-redshift galaxies were in the U-dropout sample ($z_{\mathrm{med}} = 3.0$), seven were in the $B-$dropout sample ($z_{\mathrm{med}} = 3.2$), and four were in both samples. Meanwhile, the fraction of B-dropouts with confirmed redshifts $z > 2$ is 0.78 vs. 0.40 for U-dropouts. This underscores the importance of the $B - V/V - I$ color criterion's sensitivity, both to the Lyα break at $2.3 < z < 3.3$ and to the Lyman continuum break at $3.4 < z < 4.7$.

Apart from hd4_1229_1791 at $z = 0.483$ (and hd2_1918_1912, the Galactic star), there is no evidence for redshifts lower than $z = 1.3$ or higher than $z = 5$; this includes the 12 galaxies *not* in the confirmed sample (with the possible exception of hd2_0853_0319, which resembles hd4_1229_1791 in morphology and color). If any other galaxies in our sample had $z < 1.3$, we would expect to see features such as [O II] $\lambda3727$ or the 4000 Å break. If any had $z > 5$, no flux should be visible below 5500 Å due to absorption below the Lyman continuum break, while in fact flux is visible below that wavelength in all cases. Each galaxy's red spectrum was inspected for additional emission lines or other spectral features that might support or refute the redshift assigned on the basis of the blue spectrum; no such features were found.

To investigate the galaxies' spectral properties further, we added together the spectra of all the confirmed high-redshift objects to produce a rest-frame average spectrum, shown in Fig. 4. In addition to the strong Lyα continuum break and the stellar and interstellar absorption lines mentioned above, the average spectrum shows absorption due to Lyγ, Lyβ, and Fe II $\lambda1608$, and weak emission corresponding to C III] $\lambda1909$ (although we note that the signal at the two ends of the average is dominated by only a few objects, due to the different rest-frame spectral ranges covered by the individual spectra). The latter feature is commonly seen in the spectra of active galactic nuclei (AGN), but it is also associated with planetary nebulae. The high-ionization lines of N V, Si IV, and C IV may hold some clues to the metallicity and stellar content of high-redshift star-forming galaxies; this is discussed in §5 below.

Fig. 5 shows redshifts vs. $I_{814,AB}$ for the confirmed sample. Also shown for comparison are (i) the faint magnitude limit of the Canada France Redshift Survey (Lilly *et al.* 1996); (ii) three lines corresponding to unevolved L*, 10L*, and 100L* based on NGC4449, a blue star-forming galaxy; (iii) two galaxies that have been interpreted as possible primeval

galaxies, IRAS 10214+4724 (Rowan-Robinson *et al.* 1991) and CNOC cB58 (Yee *et al.* 1996), although both those galaxies may be gravitationally lensed and thus magnified by up to a factor of 10; (iv) an Hα-emitting galaxy at $z = 2.5$ found near a QSO absorption-line cloud (Malkan, Teplitz, & McLean 1995, 1996); (v) the gravitationally lensed high-redshift galaxies discovered by Trager *et al.* (1996); and (vi) the five confirmed high-redshift objects in the HDF observed by Steidel *et al.* (1996b). Also included are two serendipitous objects at $2 < z < 3$ in the HDF flanking fields that were measured as part of a program to study compact objects (see Phillips *et al.* 1996 for more details).

The DEEP sample probes significantly fainter than most previous studies of high-redshift galaxies: the confirmed sample comprises objects that are barely more luminous than L* galaxies today. Note too that the confirmed sample has a median $I_{814,AB} = 25.0$, compared to the median $I_{814,AB} = 24.0$ for the 5 galaxies from Steidel *et al.* (1996b), who were restricted by bad weather to only a few hours total integration time.

It appeared from the uneven spatial distribution of high-redshift candidates on the three WFPC2 chips that there was evidence for clustering (as pointed out by Steidel *et al.* 1996b): 23 of the 46 original candidates are on WF2, 8 on WF3, and 20 on WF4. However, the redshift distribution shows that most of the apparent "clustering" on WF2 and WF4 is due to chance superposition rather than physical association. There is some hint of a group near $z = 3$: three galaxies within a circle of radius $85''$ have confirmed redshifts $z = 2.980, 2.990,$ and 2.991 (including iw2_0547_0293, one of the compact objects from the Flanking Field sample of Phillips *et al.* 1996). These values translate to $\sim$ 1 Mpc and a rest-frame velocity spread of $\sim$ 3300 km s^{-1}, comparable to that in dense regions (clusters or walls) of galaxies at the current epoch, and to another possible group in the HDF pointed out by Steidel *et al.* (1996b).

Several workers have used the observed colors of galaxies in the HDF to assign "photometric redshifts" and thus attempt to identify high-redshift candidates in a variation on the techniques used to select the present sample (Clements & Couch 1996; Lanzetta, Yahil, & Fernández-Soto 1996; Madau *et al.* 1996; Mobasher *et al.* 1996). Column 7 of Table 2 indicates where those studies overlap with our sample. We have compared the redshift predictions of Lanzetta *et al.* 1996 with our confirmed observed redshifts, including the Galactic star and the galaxy at $z = 0.483$, and find that there is a rough correlation with an offset $z_{DEEP} - z_{Lanzetta} = 0.35$ and an rms dispersion of 0.29 in z, not including one outlier at $z > 3$ that was predicted to have $z < 0.25$.

In Fig. 6, we plot the colors of the eleven confirmed high-redshift galaxies and compare them to the regions of color-color space chosen by Madau *et al.* (1996) to select high-redshift candidates. There are five objects – almost half our sample – that do not satisfy those

criteria and yet are confirmed to have $z > 2.9$. The criteria chosen by Madau *et al.* were designed to be efficient but also relatively free from contamination by low-redshift galaxies. Nevertheless, the regions of color-color space from which we drew our sample seem reasonably well-separated from the remainder of the HDF field galaxies at the magnitudes accessible by spectroscopy at Keck, and our contamination was limited to one Galactic star and one galaxy at $z = 0.483$. These differences demonstrate that the techniques used by Madau *et al.* and Lanzetta *et al.* are promising but not yet secure; some additional experimentation with color selection and calibration of the photometric redshift assignments using the present data will no doubt help refine the techniques.

5. Intrinsic Properties and Speculations on the Nature of $z = 3$ Galaxies

5.1. Sizes, Luminosities, and Star Formation Rates

What are the $z = 3$ galaxies in the HDF, and how do they correspond to galaxies in the nearby Universe today? We have calculated absolute luminosities M_B and intrinsic half-light radii $r_{1/2}$ based on measured redshifts, apparent magnitudes and sizes in the HDF images. We assumed k-corrections derived for a young, non-evolving galaxy with constant star formation, but including a minimal amount of dust extinction ($E(B - V) = 0.1$ with an SMC-type reddening curve; "Class 1" of Gronwall & Koo 1995). These parameters are listed in Table 2 and plotted in Fig. 7, which also shows for comparison the sizes and luminosities of a large sample of nearby galaxies with a wide variety of Hubble types. In the four cases where the source was clearly separated into discrete multiple components in the HDF images, we show the parameters for both the aggregate and individual components.

Fig. 7 reveals that the HDF galaxies at $z = 3$ are intrinsically quite small, with a median half-light radius $r_{1/2} = 3.6 \ h_{50}^{-1}$ kpc and a range $1.7 < r_{1/2} < 7 \ h_{50}^{-1}$ kpc (for $q_0 = 0.05$; for $q_0 = 0.5$, values would be $\sim 40\%$ smaller). This corresponds to the sizes of large dwarf spheroidals, H II galaxies, and Compact Narrow Emission Line Galaxies (CNELGs; Koo *et al.* 1994; Koo *et al.* 1995; Guzmán *et al.* 1996), and small ellipticals and spiral bulges. However, they are quite luminous, with median absolute magnitude $M_B = -22.5 + 5 \log h_{50}$, similar to those of the brightest normal galaxies in the local Universe and ~ 1.5 magnitudes brighter than M* (Lin *et al.* 1996). It is also apparent that the $z = 3$ galaxies overlap with the bright end of the sequence defined by local HII galaxies and distant CNELGs.

Following the prescriptions of Warren *et al.* (1995) and Steidel *et al.* (1996a), which are based on the models of Leitherer, Robert, & Heckman (1995) and Kennicutt (1983), we

have used rest-frame UV luminosities to estimate star formation rates, assuming continuing star formation and a Salpeter IMF with an 80 $M_\odot$ upper mass cutoff. SFRs for *total* objects (not subclumps) range from 7 to 25 $h_{50}^{-2}M_\odot$ yr^{-1} for $q_0 = 0.05$ (or 3 to 8 $h_{50}^{-2}M_\odot$ yr^{-1} for $q_0 = 0.5$). These values span the range found in late-type spiral and HII galaxies today (Kennicutt 1983; Gallego *et al.* 1995; Telles 1995). They are somewhat lower than the star formation rates reported by Steidel *et al.* (1996a,b; typically $SFR \sim 25h_{50}^{-2}M_\odot$ yr^{-1} for $q_0 = 0.05$), which simply reflects the fainter continuum levels reached in our sample.

Note that we have not applied any extinction correction to the rest-UV fluxes observed in the F300W and F450W filters; including an SMC-type extinction law with $E(B - V) = 0.1$ will produce about 1 magnitude of extinction at 1500 Å (Gronwall & Koo 1995; Bouchet *et al.* 1985), which would make the star formation rates higher by more than a factor of 2.

The star formation rates quoted above would produce, in the absence of absorption, Lyα emission lines with rest equivalent widths on the order of 100 Å (Charlot & Fall 1993) and observed fluxes on the order of 1×10^{-16}erg s^{-1}cm^{-2} (assuming Case B recombination and the relations calculated by Kennicutt 1983). These are well above the detection thresholds of recent searches for Lyα emission in "blank sky" (Lowenthal *et al.* 1991; Thompson & Djorgovski 1995). The low or undetected equivalent widths of Lyα emission observed in all objects in our sample (median for seven detections is $W_0 = 12$ Å) imply that there is significant internal absorption, presumably due to small amounts of dust, and demonstrate why the blank sky searches have been uniformly unsuccessful at detecting high-redshift galaxies.

Lyα emission has also been especially elusive from damped Lyα QSO absorption line clouds at high redshift, despite extensive searches (see Lowenthal *et al.* 1995 for a summary, and Djorgovski *et al.* 1996 for a recent detection). The spectra in our confirmed sample and in the somewhat brighter samples of Steidel *et al.* (1996 a,b) seem to show a damped Lyα absorption profile, on average (see Fig. 4), so we can assume that these galaxies have a sufficiently high cross-section of neutral hydrogen to cause damped Lyα absorption in QSO spectra as well. Thus the Lyman-break-selected galaxies are probably a subset of the damped Lyα clouds. The weak or absent Lyα emission lines in our current sample are entirely consistent with the upper limits and weak detections reported from damped Lyα cloud searches.

The six Lyα emission lines have FWHMs ranging from 5 to 10 Å, which, after subtracting quadratically the instrumental FWHM of 3.4 Å and correcting to rest-frame values of velocity dispersion σ, correspond to a range $100 < \sigma < 230$ km s^{-1} ($\sigma_{med} = 150$ km s^{-1}), with an estimated uncertainty on the order of 20%. The highest SNR

Lyα emission line (SNR ~ 15) has the lowest measured velocity dispersion ($\sigma = 100$ km s^{-1}) in that range. The implications and possible systematic effects are discussed in the following section.

We may draw some inferences on the physical properties of high-redshift galaxies based on the absorption lines as well. The Si IV and C IV absorption lines seen in the average spectrum in Fig. 4 are typically associated with hot stars and stellar winds, but they also arise in the interstellar medium (ISM; *e.g.*, York *et al.* 1990; Leitherer *et al.* 1996). The narrow profiles we observe in our average spectrum certainly resemble those observed in a star cluster in NGC 1705 that has an age > 10 Myr and no O stars (Leitherer 1996; Meurer *et al.*1992) more than they do the deep, stellar wind-broadened profiles seen in NGC 1741, the comparison starburst/WR galaxy shown in Fig. 2.

Furthermore, Walborn *et al.* (1995) found that early O V stars in the Small Magellanic Cloud (SMC), which has low metallicity ([Fe/H] $= -0.65$; Russell & Bessell 1989), generally exhibit significantly weaker and narrower C IV, N IV, and N V stellar wind absorption profiles than their counterparts in the higher metallicity Large Magellanic Cloud (LMC; [Fe/H] $= -0.30$), although the physical correlation is not well-established. Presumably the difference in line strengths is due to the lower terminal velocities that a low-metallicity environment produces in a radiation-driven wind. The N V, Si IV, and C IV absorption lines in our spectra of $z \sim 3$ galaxies resemble the lines in the spectra of SMC stars more than those of the LMC stars. If the absorption lines do indeed arise in the atmospheres of hot stars and not the ISM, then those stars are apparently low metallicity, consistent with an early stage of star formation.

5.2. Evolution, Masses, and Space Densities

Fig. 7 may provide some insight into the eventual fate of the high-redshift galaxies by indicating what will happen as they evolve with cosmic time. Under the assumptions that they do not undergo significant merging and that their current bursts of star formation fade in the future, they will simply move down in the $M_B - r_{1/2}$ diagram, retaining their current size. Using updated versions of Bruzual & Charlot's (1993) spectral synthesis galaxy evolution code, we calculated the evolution of a 10^7 yr burst model assuming a Salpeter IMF with stellar masses 0.1 - 125 M$_\odot$ and passive evolution. From $z = 3$ to $z = 0$, the expected amount of fading is ~ 5 mag. This would place the $z = 3$ galaxies close to the region occupied by dwarf spheroidal and irregular galaxies and spiral bulges today, but not near normal massive ellipticals or total spiral half-light radii.

If the bright cores of UV-luminous star-forming regions that we are now observing reside in the centers of larger accumulations of older, evolved populations of stars, then the apparent half-light radii will grow somewhat as the core fades. However, in H II galaxies and IR-selected starburst galaxies this effect typically amounts to only a factor of two increase in $r_{1/2}$ (Lehnert & Heckman 1996), still failing to reconcile the objects we observe at $z = 3$ with normal, massive spiral and elliptical galaxies today. Deep near-IR photometric images, such as those recently obtained by the HDF team at the Kitt Peak National Observatory 4-m telescope and those planned by the NICMOS team with HST, will help address that issue by revealing any massive, evolved stellar populations underlying the high-redshift galaxies. The possibility of growth in $r_{1/2}$ through mergers is discussed in §5.3 below.

Steidel *et al.* (1996a,b) and Giavalisco *et al.* (1996) have suggested that $z \sim 3$ U-dropout galaxies, including those in the HDF, may represent the cores of proto-spheroids that are forming stars at the centers of deep, *massive* potential wells. They cite as evidence the apparently smooth, compact morphologies in their sample, the agreement between the half-light radii of the high-redshift galaxies and those of spheroids today, and the high equivalent widths of the saturated interstellar UV absorption lines, which they tentatively interpret as implying virial velocities on the order of 200 km s^{-1}, consistent with massive galaxies. The confirmed high-redshift galaxies in the DEEP sample also show sizes similar to those of spheroids today, where by spheroids we mean the dynamically relaxed, pressure-supported portions of disk galaxies, including bulges and halos, and of ellipticals.

However, our sample of confirmed (and also candidate) high-redshift galaxies in the HDF is far from homogeneous morphologically, suggesting instead that we are observing a diverse range of physical processes or stages of formation and assemblage of galaxies. As proposed by Van Den Bergh *et al.* (1996), this discrepancy may be due at least in part to the shallower depths compared to the HDF reached in previous HST images, which would then tend to show only the brightest, most compact, and possibly most uniform features.

Furthermore, as pointed out by Conti *et al.* (1996), the large equivalent widths of saturated interstellar lines in such galaxies as NGC 1741, the starburst galaxy whose spectrum closely resembles those of our sample, cannot be used to measure masses with any certainty; this is because the lines may be broadened by such processes as supernova winds and shocks, rather than simply by virial motions. In fact, the average rest equivalent width of the unblended interstellar absorption lines in NGC 1741 is 2 Å; if the line widths reflect virial motions, this translates to a velocity width $\sigma \sim 200$ km s^{-1} or a gravitational mass $> 10^{11}$ M$_\odot$. However, the gas mass is only $M(HI) = 10^{10}$ M$_\odot$ (Williams, McMahon, & Van Gorkom 1991) and the total mass is probably $M_{tot} \ll 10^{11}$ M$_\odot$. Such equivalent widths are typical of those in the high-redshift sample, so caution should be exercised in deriving virial

masses – and broader cosmological conclusions (*e.g.*, Mo & Fukugita 1996) – therefrom.

At the same time, the small widths of the six Lyα emission lines we observe $(100 < \sigma < 230$ km s$^{-1})$ imply upper limits to gravitational masses on the order of 10^{10}M$_\odot$, small in comparison to massive galaxies today. This mass constraint may be more robust than the absorption line equivalent widths, since most radiative transfer effects act to broaden Lyα, although Lyα emission is certainly complex and may be asymmetrically absorbed or originate in only a small fraction of the total star-forming area (*e.g.*, Auer 1968; Neufeld 1991; Charlot & Fall 1993).

One exception may be the case of C4-09 – the unusual four-knot system of Steidel *et al.* (1996b). We confirm the result of Zepf *et al.* (1996) that the Lyα emission line is clearly resolved into two components separated by 14 Å, or 820 km s^{-1} in the rest frame[6] (Fig. 2). We can use this separation to estimate the mass of the system under the assumption that the split is due to gravitationally-induced motions. The slitlet was aligned at $PA = 137°$, constrained by the two candidate galaxies on either side of C4-09. The longest projected separation of the four knots of emission along the slit, then, is $0\rlap{.}''9$ or ~ 11 h_{50}^{-1} kpc $(q_0 = 0.05)$ (although the seeing disk smeared the image sufficiently that our spectrum has no spatial information). For a circular velocity of 100 km s^{-1} at a radius $r = 5.5$ kpc, we then infer a gravitational mass of $\sim 2 \times 10^{11}$ M$_\odot$, comparable to local massive galaxies.

The moderate star formation rates implied by the UV fluxes may be difficult to reconcile with the rapid, early formation of massive spheroids usually inferred from stellar population studies of local galaxies (*e.g.*, Bower, Lucey, & Ellis 1992). At a constant star formation rate of 10 M$_\odot$ yr^{-1}, the high-redshift HDF galaxies would require 10^{10} yr to produce a 10^{11} M$_\odot$ spheroid. Conversely, the mass-to-light ratios for active starbursts are as low as $M/L = 0.1$ (Guzmán *et al.* 1996), implying typical masses $M \sim 10^{10}$ M$_\odot$ for our calculated luminosities.

More clues to the nature of the $z = 3$ galaxies come from their space density compared to local galaxies today. Considering only the 11 confirmed high-redshift galaxies presented here plus the 5 observed by Steidel *et al.* (1996b) yields at least 16 objects in the range $2.2 < z < 3.5$ in the HDF. The 4.7 arcmin^2 field constitutes a volume of 68000 h_{50}^{-3} comoving Mpc^3 for $q_0 = 0.05$ or 14000 h_{50}^{-3} Mpc^3 for $q_0 = 0.5$ over that redshift range, so the space density of high-redshift star-forming galaxies is $n \geq 2.4 \times 10^{-4}$ h_{50}^3 Mpc^{-3} for $q_0 = 0.05$ or $n \geq 1.1 \times 10^{-3}$ h_{50}^3 Mpc^{-3} for $q_0 = 0.5$. The latter value is close to twice the density of $L \geq$ L* galaxies in the local Universe, $n(L \geq$ L$^*) = 6 \times 10^{-4}$ h$_{50}^3$Mpc^{-3} (where

---

[6]Note that we find redshifts $z = 3.210, 3.222$, somewhat lower than the redshift $z = 3.226$ reported by Steidel *et al.* but in good agreement with Zepf *et al.*

we have integrated the bright end of the luminosity function derived by Lin *et al.* 1996 from the Las Campanas Redshift Survey), and 3 - 4 times higher than the values found by Steidel *et al.* (1996a) from ground-based UGR photometric selection and Keck spectroscopy of a slightly brighter sample. This higher density reflects the additional 1 magnitude of depth in our sample; the additional confirmed U-dropouts; and the B-dropouts, which alone provided 27% of our confirmed sources, not including those objects that were also U-dropouts.

If the 16 objects we did *not* observe (due to time constraints), which have a color and magnitude distribution similar to the observed sample, also have a 44% success rate of redshifts $2.2 < z < 3.6$, the additional seven high-redshift objects would boost the number density in the HDF by almost 50%. Furthermore, since none of the non-confirmed objects we observed is inconsistent with being in that redshift range, the total list of 46 high-redshift candidate galaxies could yield a number density as much as three times higher than the figure quoted above. If indeed all of these sources are the precursors of today's $L > L^*$ ellipticals and spheroids of spirals, then substantial merging and/or fading must have taken place between then and now to reduce their numbers and reconcile them with the local luminosity function.

Lanzetta *et al.* (1996) estimate the surface densities of galaxies in the HDF as a function of redshift and apparent magnitude based on their photometric properties. The surface density of the DEEP sample of confirmed high-redshift galaxies, coupled with Steidel *et al.*'s (1996b) and normalized to 1 arcmin^2, agrees reasonably well with those estimates except in the lowest of the three redshift bins we targeted. For $I_{814,AB} < 26$, the predictions are $8.1 \pm 0.7, 1.9 \pm 0.3$, and 2.1 ± 0.3 galaxies arcmin^{-2} in the redshift ranges 2.0 - 2.5, 2.5 - 3.0, and 3.0 - 3.5, respectively. We find 0.6, 1.5, and 1.3 confirmed galaxies arcmin^{-2} in those ranges, consistently below the 1σ error boundary, but since we expect many or most of the unconfirmed galaxies also to lie in those ranges, the actual surface densities probably match or even exceed the estimates of Lanzetta *et al.* in the higher redshift bins.

The integrated star formation rate for the 11 confirmed high-redshift galaxies is $SFR = 200~h_{50}^{-2}~\mathrm{M_\odot~yr^{-1}}$ ($q_0 = 0.05$) or $72~h_{50}^{-2}~\mathrm{M_\odot~yr^{-1}}$ ($q_0 = 0.5$) in the volumes quoted above. This amounts to $2.9 - 5.1 \times 10^{-3}h_{50}^{-1}~\mathrm{M_\odot~yr^{-1}Mpc^{-3}}$ (for $q_0 = 0.05 - 0.5$), about 10 - 15% of the local value of $0.04~\mathrm{M_\odot~yr^{-1}Mpc^{-3}}$ measured by Gallego *et al.* (1996; note that we have divided the integrated SFR from Gallego *et al.* by 3.3 to transform from a Scalo IMF to a Salpeter IMF, *e.g.*, Kennicutt 1983). If we include the objects from Steidel *et al.* (1996b), the measured integrated SFR at $z = 3$ approaches one-half the local value for $q_0 = 0.5$; including the extinction correction mentioned in §5.1 would bring the two values into rough equilibrium. The $z = 3$ value is still an order of magnitude lower than the star

formation density measured at $z = 1$ by Lilly *et al.* (1996) from the CFRS, but of course the $z = 3$ estimate is a lower limit based only on the bright end of the luminosity function of star-forming galaxies at $z = 3$; as Gallego *et al.* show for the local Universe, as much as 90% of the integrated SFR can come from the faint end ($L < L_\alpha^*$) of the Hα luminosity function.

There is a hint from the 16 confirmed high-redshift objects in the HDF (the present sample plus that of Steidel *et al.* 1996b) of luminosity or density evolution with redshift. If we divide the combined samples into three redshift ranges 2.20 - 2.68, 2.68 - 3.11, and 3.11 - 3.50, each with volume $V \sim 22,000\ h_{50}^{-3}\mathrm{Mpc}^3$ ($q_0 = 0.05$), then we find 4, 6, and 6 objects, respectively, in each bin. However, if we restrict the sample to the 12 objects brighter than $M_B = -22.3$, then we find only one object in the low-redshift bin, but six and five objects in the medium- and high-redshift bins, respectively. This suggests that luminous star-forming galaxies have either faded or merged or both during the ~ 2 Gyr (for $q_0 = 0.05, H_0 = 50$ km s^{-1}Mpc^{-1}) between $z = 3.5$ and $z = 2.2$. Alternatively, they may progressively extinguish their UV light as massive stellar processing causes an increase in metallicity and dust. Clearly this will be a fascinating line of inquiry to pursue with larger datasets that sample more densely the luminosity function at high redshift.

5.3. A Low-Mass Starburst Scenario

To help guide the discussion and interpretation of the star-forming galaxies at $z \sim 3$ in the HDF, including those observed by Steidel *et al.* (1996b), we summarize their salient observed characteristics and then speculate on the ultimate fate of these distant galaxies and their possible connections to normal galaxies in the local Universe:

- Typical B-band luminosities are 1 - 2 magnitudes brighter than present day L*.

- Median half-light radius is small: $r_{1/2} = 3.6 h_{50}^{-1}$ kpc for aggregate systems and $r_{1/2} = 2.7 h_{50}^{-1}$ kpc for subclumps ($q_0 = 0.05$; smaller by 0.6 times for $q_0 = 0.5$).

- Morphologies are varied, with multiple knots of emission and diffuse wispy tails that imply non-relaxed systems.

- Star formation rates are modest: 7 - 24 h_{50}^{-2}M$_\odot$ yr^{-1} for $q_0 = 0.05$ (3 - 9 h_{50}^{-2}M$_\odot$ yr^{-1} for $q_0 = 0.05$; not corrected for dust extinction).

- Lyα emission is weak when it is present at all, and the observed profile is narrow, $FWHM_{\mathrm{med}} = 7$ Å, implying $\sigma_{\mathrm{med}} = 140$ km s^{-1}.

- Stellar and interstellar absorption lines of heavy elements are similar to those seen in the spectra of nearby starburst and WR galaxies, but narrow, weak stellar-wind profiles and equivalent widths may imply low metallicity.

- The comoving volume density, including the 5 objects reported by Steidel *et al.* (1996b), is $n \geq 2.5 \times 10^{-4} h_{50}^3 \mathrm{Mpc}^{-3}$ for $q_0 = 0.05$, or $n \geq 1.2 \times 10^{-3} h_{50}^3 \mathrm{Mpc}^{-3}$ for $q_0 = 0.5$, comparable to the local volume density of galaxies with $L > \mathrm{L}^*$. The volume density could be 3 - 4 times higher if most of the remaining candidates are also at $2.2 < z < 3.5$.

- Strong clustering is not observed.

- Star-forming galaxies are seen from $z = 2.2$ to $z = 3.5$, the range to which our study was sensitive; the redshift distribution appears to be slightly weighted towards higher redshifts.

We consider three possible scenarios of galaxy formation and evolution that might explain the present observations. In the first scenario, the luminous, compact, star-forming objects we observe represent the *cores* of *massive* spheroids of today's $L > \mathrm{L}^*$ elliptical and spiral galaxies. In this picture, which is perhaps similar to what Steidel *et al.* (1996a,b) have proposed, the sites of star formation lie near the centers of deep potential wells that are continuously funnelling in new gas and processing it into stars at roughly 10 $\mathrm{M_\odot}$ yr^{-1} for many Gyr, eventually building a stellar mass $M \sim 10^{10}$ $\mathrm{M_\odot}$. In support of such a view is the apparent agreement between the half-light radii of high-redshift galaxies and those of local spheroids and bulges, as noted above, and the similar comoving number densities of high-redshift galaxies and $L > \mathrm{L}^*$ galaxies today.

It seems clear from the HDF redshift distribution that the high-redshift population is a *field* population, not the precursor of clusters. The random statistics of probing high redshifts favor field galaxies overwhelmingly in any case. That, together with the large number density, suggests that if they are indeed forming spheroids, then these objects are not the spheroids of massive ellipticals but rather the spheroids/bulges of early-type spirals. This is consistent with the half-light radii, which match those of local bulges but are smaller than those of giant ellipticals (*e.g.*, Bender et al. 1992).

However, the size agreement may be somewhat superficial: If these early phases of galaxy evolution show low-metallicity stars, analogous to Pop II stars in the Milky Way, then we should properly compare with the radii of local Pop II components. This is larger than $r_{1/2}$ given above – in the Milky Way, for example, the Pop II component of globular clusters with $Z < 0.1$ has a median radius of 10 kpc (Harris and Racine 1979) and

extends to ~ 50 kpc, very much larger than the median half-light radius $r_{1/2} = 3.6$ kpc we observe for even the *aggregate* systems. The number density agreement may be somewhat superficial as well, since significant merging can easily cut the numbers by factors of several and/or induce additional luminous bursts of star formation, and passive fading of the stellar components can dim the objects by 5 magnitudes (see previous section).

A second possible scenario borrows from models of hierarchical clustering, which predict that highly overdense systems like those believed to form spheroids and bulges (Blumenthal et al. 1984) begin to collapse with many subclumps (Kauffmann, White, & Guiderdoni 1993; Navarro, Frenk, & White 1995; Cole *et al.* 1994). A subclump model has also been advanced by Searle and Zinn (1978) for the formation of the metal-poor spheroid of the Milky Way. We might therefore expect to see a *population* of subclumps in every high-redshift proto-spheroid, distributed over a volume $\gtrsim 10$ kpc in radius , or 1 - 2$''$ on the sky. This is not in general seen (although there are a handful of cases in which companion blobs at radii $\sim 1 - 2''$ have colors that suggest similar redshift). This seeming contradiction might be accounted for if the bright phase of each individual blob lasted for only a few $\times 10^8$ yr, so that, on average, only one blob is seen at any one time. We then have what might be termed a "Christmas tree" model, wherein small individual star-forming blobs come and go within a much larger – and largely invisible – spheroid structure. It will be important to gather dynamical evidence to test this picture.

Finally, we suggest a third alternative in which the $z = 3$ galaxies are relatively low-mass *isolated* knots of star formation similar to current-day H II galaxies, 10 - 100 times less massive than typical L* disk spheroids or ellipticals. In this scenario, rather than forming stars at a steady rate over many Gyr, the galaxies at $z = 3$ would be converting gas to stars in small components through more intense bursts with low mass-to-light ratios, such as the CNELGs observed at lower redshifts with $M/L \sim 0.1$ (Guzmán *et al.* 1996). This would naturally explain the apparently high number density of galaxies at $z = 3$ in the HDF, since relatively low-mass objects would be easily included in our sample due to their intense brightness. The diffuse, wispy tails and diverse morphologies of many of our sample sources indicate that a large supply of gas is generally available for future star formation nearby; as star formation progresses in the luminous, compact knots, gas may be used up locally or expelled through supernova-driven winds (e.g. Guzmán *et al.* 1996; Lehnert & Heckman 1996), star formation may taper off exponentially, and new regions of star-forming activity may spring up in other dense pockets of gas. The end products of such a process could be low-mass spheroidal galaxies such as those observed in the Local Group. The diverse morphologies, moderate star formation rates, and small sizes all seem to favor the "Christmas tree" picture or this low-mass burst scenario.

Of course, the actual picture may be some combination of those three descriptions: extensive merging of clumps could produce a wide range of galaxy types and masses by the present epoch. Such a scenario is supported by recent N-body and semi-analytical models of galaxy formation and evolution (*e.g.*, Kauffmann & White 1993), which favor complex and rich merging histories for most massive galaxies. The small individual knots that we observe within regions only a few kpc across in four confirmed high-redshift systems are also likely to merge soon: even assuming a mass-to-light ratio as low as $M/L = 0.1$, appropriate for an intensely star-forming system (Guzmán *et al.* 1996), the dynamical time for an L* object 3 kpc across is ~ 0.1 Gyr.

One important caveat to keep in mind when interpreting rest-UV morphologies, of course, is that those morphologies may bear little resemblance to the rest-optical view of galaxies with which we are familiar in the local Universe. Even "grand design" spiral galaxies often display barely recognizable, scattered clumps of star-forming regions when observed at 1200 Å (O'Connell & Marcum 1996). We are certainly observing only the most intense bursts of star formation at the location and epoch surveyed by the HDF; there are, no doubt, complex underlying mass structures and fainter star formation sites lurking below our current detection limits.

We cannot measure the masses of $z = 3$ galaxies directly given the present data. Therefore, while we find no direct evidence that the $z = 3$ galaxies discussed here are massive ($M > 10^{10} M_\odot$), there is also no evidence that they will not eventually merge with similar objects to *become* massive galaxies today. In any case, whether any of these particular explanations is correct, it is clear that the morphologies, sizes, spectra, and numbers of the high-redshift galaxies contain key information on the structure of proto-galaxies.

Database (NED), which is operated by the Jet Propulsion Laboratory, Caltech, under contract with the NASA.

A. Notes on individual objects

Listed in order of increasing Right Ascension, as in Table 1.

A.1. hd4_0259_1947

A clearly disk-shaped galaxy $2''$ from a larger and brighter disk. The object is barely visible in the F300W image, but is a solid $U-$dropout, implying $z > 1.7$ (for a Lyα break) or, more likely given the large $U - B$ color, $z \gtrsim 2.6$ (for a Lyman continuum break). If confirmed to be at such a high redshift, this would certainly be one of the earliest-formed disk systems known. The larger disk nearby is considerably redder and therefore probably at lower redshift.

A.2. hd4_1076_1847

The brightest galaxy in the sample, but uncertain redshift. Mg II absorption at $z = 0.879$ and $z = 1.010$ is detected in the spectrum (cf. §4), presumably due to the galaxies at those redshifts 1-2$''$ to the west and south, respectively. The spectrum shows no definite Lyα break or emission lines above 4580 Å, so the redshift is most likely $1.01 < z < 2.8$. There is a possible weak emission line at 5433 Å. The color matches that of confirmed galaxies at $z \sim 2.5$; the absorbing galaxies at $z = 0.879$ and $z = 1.010$ have very different colors. After removing the Mg II absorption lines from the spectrum, we find a cross-correlation peak at $z = 2.41$, but no other features to confirm that redshift. A weak absorption lines at 4884 Å could match C IV $\lambda1550$ at $z = 2.15$ (or Al II at $z = 1.93$), however, and we adopt that as a tentative redshift.

A.3. hd4_1229_1791 ($z = 0.483$)

A diffuse, low-surface brightness galaxy; the only object in the sample with a confirmed redshift $z < 2$. The source is only $4''$ and $7''$ from galaxy C4-09 at $z = 3.22$ of Steidel *et al.* (1996b) and hd4_1076_1847 at $z \geq 1$, respectively. Evidently the 4000 Å break, redshifted to ~ 6000 Å, allowed the object to be included in the $B-$dropout sample. The single emission line in the blue spectrum (shown in Fig. 2) is apparently [O II] $\lambda3727$, with a rest equivalent width $W_{[OII]} = 39$Å. The red spectrum shows possible Hβ and faint [O III] $\lambda5007$ emission lines, and the strong U-band detection ($U_{300,AB} = 26.86$) further demonstrates that the redshift must be $z < 2.6$.

A.4. hd2_2030_0287 ($z = 2.267$):

We identify the strong emission line as Lyα; weak absorption lines match the expected wavelengths of Si II, C II and C IV. If the emission line were [O II] $\lambda 3727$ at $z = 0.066$, the absolute magnitude would be $M_B \sim -11.7$ and the [O II] rest equivalent width would be $W_0 > 100$ Å, high compared to local samples (*e.g.*, Terlevich *et al.* 1991; Broadhurst, Ellis, & Shanks 1992) although not implausible.

A.5. hd4_0818_1037

The spectrum shows reasonably strong continuum with a strong absorption line at 5066 Å, identified by Cohen *et al.* (1996) as C IV $\lambda 1550$ at $z = 2.268$. However, no other features matching that redshift are evident, and we list in Table 2 a tentative alternate redshift $z = 2.035$ based on the best peak of the cross-correlation *with the combined spectrum shown in Fig. 4*; this corresponds to the absorption line being Al II.

A.6. hd2_1881_0374

This isolated, compact source shows a healthy $U - B$ break but is detected in the F300W image, so the redshift is most likely $z < 2.6$. The spectrum shows some broad features but we were unable to identify any with certainty.

A.7. hd4_1994_1406

Although the cross-correlation peak for this compact galaxy is at $z = 3.630$ – higher than any other object in the sample, confirmed or unconfirmed – we regard this redshift as suspect since the object is detected in the F300W image.

A.8. hd2_1410_0259 ($z = 3.160$)

A complex source with a bright asymmetrical core and extended plumes of emission, all with roughly the same color. We identify the emission line as Lyα, and there is good agreement with weak absorption lines matching Si II, O I, and C II. If the emission line were instead [O II] $\lambda 3727$ at $z = 0.359$, then we would expect to see Hβ and [O III] $\lambda 5007$

in the blue spectrum and/or Hα in the red spectrum; no such lines are seen (although the red spectrum is heavily contaminated by night sky emission lines).

A.9.   hd4_1486_0880

One of the most symmetrical profiles in the sample. The best peak of the cross-correlation with the spectrum of NGC 1741 is at $z = 2.952$, but we list instead $z = 2.47$ based on the general shape and possible agreement with a few stellar and interstellar absorption lines.

A.10.   hd2_0853_0319

A very faint, diffuse galaxy, with almost undetectable continuum and no emission lines or strong breaks in the blue or red spectrum. The cross-correlation function peaks at $z = 3.35$, but the object is weakly detected in the F300W filter, so it may in fact lie at $z < 2.6$; the morphology and color are indeed similar to those of hd4_1229_1791 ($z = 0.483$), the only galaxy with a confirmed redshift $z < 2$.

A.11.   hd4_0367_0266 ($z = 2.931$)

Two nearly equal knots of emission are roughly aligned with a clumpy, diffuse tail, all of approximately the same color. The broad Lyα absorption trough, strong Lyα break, and strong, sharp absorption lines of many interstellar and stellar ions provide a secure redshift. The disk galaxy a few arcsec to the southwest has a different color and therefore probably a significantly different redshift.

A.12.   hd4_2030_0851 ($z = 2.980$)

The least secure of the confirmed subsample. The redshift is based on the break at 4850Å, which we identify as Lyα, and is supported by weak absorption line matches with the wavelengths expected for Si II 1526Å and C IV 1550Å and by the object's non-detection in the F300W filter. The object $1''$ to the northeast is almost certainly at lower redshift, judging from its red color.

A.13. hd4_1341_0299

A compact object with a close companion of considerably different color, and therefore probably a chance projection rather than physical association. The spectrum shows one possible weak emission line at 5334Å, which could match Lyα at $z = 3.379$, but no Lyα break or interstellar absorption lines are present; we list in Table 2 $z = 2.31$ based on a peak in the cross-correlation function (a weaker peak appears at $z = 3.35$).

A.14. hd2_1739_1258

Morphologically the most complex object in the sample. Numerous bright knots and filaments with a broad range in color are arranged in a rough line $3''$ long, and a redder clump of emission – possibly at different redshift – lies only $1''$ to the west. Our spectrum was obtained with the slitlet aligned with the object's major axis. Despite the object's relative brightness, the blue spectrum failed to reveal any identifiable features. The red spectrum shows a possible faint emission line at 6850 Å that would match [O II] $\lambda3727$ at $z = 0.838$, but no other features support that redshift, and the line is not convincing. We adopt $z = 2.72$, the cross-correlation peak that provides the best matches with Lyα and C IV $\lambda1550$ absorption.

A.15. hd3_0408_0684 ($z = 3.233$)

We identify the strong emission line as Lyα. No absorption lines are detected, but there is a clear break across the emission line and a strong $U-$band limit that support the identification.

A.16. hd2_1410_1282

The faint continuum in our spectrum yielded no secure features; the redshift listed in Table 2 is from the cross-correlation spectrum, supported by the large $U - B$ color.

A.17. hd2_0698_1297 ($z = 3.430$)

The highest reliable redshift in the sample is based on the Lyα emission line and continuum break, and good matches of absorption lines with Si II and O I. The Lyα line appears slightly redshifted ($z = 3.439$, perhaps due to internal self-absorption) with respect to the absorption lines, which we use to derive the exact redshift. The images show two close knots of emission adjacent to a wispy cloud, all with similar colors. The source is only $4''$ (48 h_{50} kpc, $q_0 = 0.05$) projected separation from hd2_0705_1366 ($z = 3.368$), but the redshift difference corresponds to more than 20,000 km s^{-1} in the rest frame, so the likelihood of physical association is low. However, there are two possible absorption lines in the spectrum that show rough agreement with Si II $\lambda 1260$ and O I $\lambda 1303$ at $z = 3.368$, presumably due to hd2_0705_1366.

A.18. hd2_0705_1366 ($z = 3.368$)

The strong emission line and break are almost certainly Lyα. A possible weak absorption line at 4482 Å matches the wavelength expected for Lyβ at the Lyα emission redshift, but the continuum is extremely weak here and the absorption line is probably spurious. Despite some faint extended emission, the bright core gives this galaxy the smallest half-light radius in our sample, $r_{1/2} = 0''.14$, indistinguishable from a point source.

A.19. hd2_1918_1912

A Galactic star, also observed by Steidel *et al.* (1996); it was included in our sample through an oversight of that fact.

A.20. hd2_0434_1377 ($z = 2.991$)

This compact, slightly elongated source shows the strongest absorption lines in the sample. The Lyα, Si II, O I, and C II absorption lines make the spectrum virtually identical to that of NGC 1741, the local comparison starburst galaxy used in the cross-correlations.

A.21. hd2_1359_1816 ($z = 3.181$)

The redshift is based on the excellent agreement of the clear break at 5100Å with Lyα and of several strong absorption lines with common UV stellar and interstellar features.

A.22. hd2_0624_1688 ($z = 2.419$)

Three very close knots of emission are contained within $1''$. The redshift is based on the Lyα line; no absorption lines are detected. Since no other emission lines are visible in either the blue or red spectrum, the only other plausible assignment for the emission line – [O II] λ3727 – is highly unlikely.

A.23. hd3_1455_0430

A tight, symmetrical profile with a faint companion less than $1''$ to the north, and several objects with comparable brightness but dissimilar colors (and therefore redshifts) within $5''$. Continuum is quite strong in our spectrum, and there are two absorption lines at 5097 Å and 5648 Å, but we were unable to make a positive identification. We adopt $z = 2.644$ based on the general shape and the location of weak features matching C IV λ1550 and interstellar UV lines.

A.24. hd2_0725_1818 ($z = 2.233$)

This asymmetrical galaxy lies only $1''$ to the southwest of hd2_0743_1844, and the two sources' colors are almost identical. The excellent agreement of strong absorption lines with the wavelengths of Si II, O I, C II, and Al II and the possible emission line of C III] make the redshift assignment secure.

A.25. hd2_0743_1844

Despite the apparent similarities and proximity to hd2_0725_1818, this galaxy's spectrum yields no secure features. We adopt the redshift $z = 2.390$ given by the best peak of the cross-correlation function.

REFERENCES

Auer, L. H. 1968, ApJ, 153, 783

Bahcall, J., 1991, in *The Decade of Discovery in Astronomy and Astrophysics* (Washington: National Academy Press)

Bender, R., Burstein, D., & Faber, S. M. 1992, ApJ, 399, 462

Blumenthal, G. R., Faber, S. M., Primack, J. R., & Rees, M. J. 1984, *Nature*, 311, 517

Bouchet, P., Lequeux, J., Maurice, E., Prevot, L., & Prevot-Burnichon, M. L. 1985, å, 149, 330

Bower, R. G., Lucey, J. R. , & Ellis, R. S. 1992, MNRAS, 254, 601

Broadhurst, T. J., Ellis, R. S., & Glazebrook, K. 1992, Nature, 355, 55

Bruzual A., G. & Charlot, S. 1993 ApJ, 405, 538

Charlot, S. & Fall, S. M. 1993, ApJ, 415, 580

Clements, D. L. & Couch, W. J. 1996, MNRAS, 280, L43

Cohen, J. G., Cowie, L. L., Hogg, D. W., Songaila, A., Blandford, R., Hu, E. M., & Shopbell, P. 1996, ApJ, 471, 5L

Cole, S., Aragón-Salamanca, A., Frenk, C. S.,, Navarro, J. F., & Zepf, S. E. 1994, MNRAS, 271, 781

Connolly, A., Csabai, I., Szalay, A. S., Koo, D. C., & Kron, R. G. 1995, AJ, 110, 2655

Conti,, P. S., Leitherer, C., & Vacca, W. D. 1996, ApJ, 461, L87

Cowie, L. L., Hu, E. M., & Songaila, A. 1995, AJ, 110, 1576

Djorgovski, S. G., Pahre, M. A., Bechtold, J., & Elston, R. 1996, *Nature*, 382, 234

Drinkwater, M. M., Webster, R. L., & Thomas, P. A. 1993, AJ, 106, 848

Ebbels, T. M. D., Le Borgne, J.-F., Pelló, R., Ellis, R. S., Kneib, J.-P., Smail, I., & Sanahuja, B. 1996, MNRAS, 281, 75L

Gallego, J., Zamorano, J., Aragón-Salamanca, A., & Rego, M. 1995, ApJ, 455, L1

Giavalisco, M., Steidel, C. C., & Macchetto, D. 1996, ApJ, 470, 189

Gronwall, C. & Koo, D. C. 1995, ApJ, 440, 1L

Gronwall, C. 1996, Ph.D. thesis, University of California, Santa Cruz

Guzmán, R., Koo, D. C., Faber, S. M., Illingworth, G. D., Takamiya, M., Kron, R. G., & Bershady, M. B. 1996, ApJ, 460, L5

Harris, W. E. & Racine, R. 1979, ARA&A, 17, 241

Kauffmann, G. & White, S. D. M. 1993, MNRAS, 261, 921

Kauffmann, G., White, S. D. M., & Guiderdoni 1993, MNRAS, 264, 201

Kennicutt, R. C. 1983, ApJ, 272, 54

Koo, D. C. 1985, AJ, 90, 418

Koo, D. C., Bershady, M. A., Wirth, G. D., Stanford, S. A., & Majewski, S. R. 1994, ApJ, 427, 9L

Koo, D. C., Guzmán, R., Faber, S. M., Illingworth, G. D., Bershady, M. A., Kron, R. G., & Takamiya, M. 1995, ApJ, 440, L49

Lanzetta, K. M., Yahil, A., & Fernández-Soto, A. 1996, Nature, 381, 759

Lehnert, M. D. & Heckman, T. M. 1996, ApJ, 472, 546

Leitherer, C. 1996, in Proc. of 33rd Liege Intl. Astroph. Colloq., in press

Lilly, S. J., Le Fèvre, O., Hammer, F., & Crampton, D. 1996, ApJ, 460, L1

Lin, H., Kirshner, R. P., Shectman, S. A., Landy, S.D., Oemler, A., Tucker, D. L., & Schechter, P. L. 1996, ApJ, 464, 60

Lowenthal, J. D., Hogan, C. J., Leach, R. W., Schmidt, G. D., & Foltz, C. B. 1991, ApJ, 357, 3

Lowenthal, J. D., Hogan, C. J., Green, R. F., Woodgate, B., Caulet, A., Brown, L., & Bechtold, J. 1995, ApJ, 451, 484

Madau, P. 1995, ApJ, 441, 18

Madau, P., Ferguson, H. C., Dickinson, M. E., Giavalisco, M., Steidel, C. C., & Fruchter, A. 1996, MNRAS, in press

Malkan, M. A., Teplitz, H., & McLean, I. S. 1995, ApJ, 448, L5

Malkan, M. A., Teplitz, H., & McLean, I. S. 1996, ApJ, 468, 9L

Marzke, R. O., Geller, M. J., Huchra, J. P., & Corwin, H. G. Jr. 1994, AJ, 108, 437

Meurer, G. R., Freeman, K., Dopita, M., & Cacciari, C. 1992, AJ, 103, 60

Mo, H. J. & Fukugita, M. 1996, ApJ, 467, L9

Mobasher, B., Rowan-Robinson, M., Georgakakis, A., & Eaton, N. 1996, MNRAS, 282, 7L

Navarro, J. F., Frenk, C. S., & White, S. D. M. 1995, MNRAS, 275, 56

Neufeld, D. A. 1991, ApJ, 370, L85

O'Connell, R. W. & Marcum, P. 1996, in *HST and the High-Redshift Universe (37th Herstmonceux Conference)*, eds. N. R. Tanvir, A. Aragón-Salamanca, J. V. Wall

Oke, J. B., *et al.* 1995, PASP, 107, 375

Phillips, A. C., Guzmán, R., Gallego, J., Lowenthal, J. D., Vogt, N. P., Faber, S. M., Koo, D. C., & Illingworth, G. D. ApJ, submitted

Rowan-Robinson, M., *et al.* 1991, *Nature*, 351, 719

Russell, S. C. & Bessell, M. S. 1989, ApJS, 70, 865

Steidel, C. C. 1995, in *QSO Absorption Lines*, p. 139 (Berlin: Springer-Verlag)

Searle, L. & Zinn, R. 1978, ApJ, 225, 357

Steidel, C. C., Giavalisco, M., Pettini, M., Dickinson, M., & Adelberger, K. L. 1996a, ApJ, 462, 17L

Steidel, C. C., Giavalisco, M., Dickinson, M., & Adelberger, K. L. 1996b, AJ, 112, 352

Telles, E. 1995, Ph. D. thesis, Univ. of Cambridge

Terlevich, R., Melnick, J., Masegosa, J., Moles, M., & Copetti, M. V. F. 1991, A&AS, 91, 285

Thompson, D. T. & Djorgovski, S. G. 1995, AJ, 110, 982

Trager, S. C., Faber, S. M., Dressler, A., & Oemler, A. Jr. 1996, ApJ, submitted

Van Den Bergh, S., Abraham, R. G., Ellis, R. S., Tanvir, N. R., Santiago, B. X., & Glazebrook, K. G. 1996, AJ, 112, 359

de Vaucouleurs, G. de Vaucouleurs, A., Corwin, H. G., Buta, R. J., Paturel, G., & Fouqué, P. 1991, Third Reference Catalogue of Bright Galaxies (New York, Springer-Verlag)

Vogt, N. P. *et al.* 1996, ApJ, in press

Walborn, N. R., Lennon, D. J., Haser, S. M., Kudritzki, R.-P., & Voels, S. A. 1995, PASP, 107, 104

Williams, R. E. *et al.* 1996, AJ, 112, 1335

Williams, B. A., McMahon, P. M. & Van Gorkom, J. H. 1991, AJ, 101, 1957

York, D. G., Caulet, A., Rybski, P., Gallagher, J., Blades, J. C., Morton, D. c., & Wamsteker, W. 1990, ApJ, 351, 412

Yee, H. K. C., Ellingson, E., Bechtold, J., Carlberg, R. G., & Cuillandre, J.-C. 1996, AJ, 111, 1783

Zepf, S. E., Moustaka, L. A., & Davis, M. 1996, ApJ, in press

TABLE 1

THE DEEP SAMPLE OF CANDIDATE HIGH-REDSHIFT GALAXIES IN THE HDF

Name[a]	RA (2000)	DEC (2000)	$I_{814,AB}$[b]	$U - B$[c]	$B - V$[d]	$B - I$[e]	class[f]	Exp.[g]
hd4_0259_1947	12:36:38.532	62:12:34.86	24.26	> 2.59	0.78	1.15	U	6
hd4_1076_1847	12:36:40.871	62:12:06.43	23.27	1.61	0.39	0.68	U	12
hd4_1229_1791	12:36:41.506	62:12:01.68	25.01	0.55	0.99	1.29	B	12
hd2_2030_0287	12:36:43.991	62:14:11.01	24.54	2.08	0.10	0.11	U	12
hd4_0818_1037	12:36:44.551	62:12:28.48	23.77	1.50	0.22	0.58	U	6
hd2_1881_0374	12:36:44.784	62:14:06.96	24.79	1.58	0.32	0.71	U	6
hd4_1994_1406	12:36:45.220	62:11:39.62	25.45	1.48	0.21	0.17	U	6
hd2_1410_0259	12:36:45.268	62:13:47.97	25.44	> 1.65	0.81	0.91	U, B	6
hd4_1486_0880	12:36:46.858	62:12:06.43	24.14	2.04	0.59	0.92	U	6
hd2_0853_0319	12:36:46.861	62:13:28.65	25.02	0.79	0.89	1.21	B	12
hd4_0367_0266	12:36:47.596	62:12:56.99	24.76	> 1.48	1.50	1.77	U, B	12
hd4_2030_0851	12:36:48.214	62:11:46.92	25.12	> 1.97	0.76	0.92	U	12
hd4_1341_0299	12:36:49.587	62:12:20.75	25.28	> 2.40	0.27	0.32	U	12
hd2_1739_1258	12:36:49.725	62:14:16.01	23.58	1.54	0.24	0.63	U	6
hd3_0408_0684	12:36:49.735	62:12:49.94	25.17	> 1.39	1.18	1.45	B	12
hd2_1410_1282	12:36:50.607	62:14:04.40	25.28	2.06	0.42	0.60	U	12
hd2_0698_1297	12:36:52.320	62:13:38.73	24.97	> 1.45	1.22	1.58	B	12
hd2_0705_1366	12:36:52.664	62:13:40.06	25.10	> 1.72	0.96	1.18	U, B	12
hd2_1918_1912	12:36:52.725	62:14:33.04	20.84	2.79	0.78	1.20	U	6
hd2_0434_1377	12:36:53.343	62:13:30.39	24.64	> 2.19	0.91	1.18	U, B	12
hd2_1359_1816	12:36:53.508	62:14:11.12	24.63	> 1.71	1.32	1.66	B	12
hd2_0624_1688	12:36:54.531	62:13:42.29	25.32	2.47	0.15	0.14	U	12
hd3_1455_0430	12:36:54.634	62:13:15.82	24.32	1.63	0.29	0.38	U	12
hd2_0725_1818	12:36:54.978	62:13:48.05	24.59	1.89	0.20	0.23	U	12
hd2_0743_1844	12:36:55.070	62:13:49.12	25.40	1.84	0.35	0.49	U	12

[a]Names are of the form hdn_xxxx_yyyy, where n is the WFPC2 chip number and xxxx and yyyy give the pixel coordinates of the object in the version 1 "drizzled" $F814W$ HDF images.

[b]$I814$ isophotal magnitude on the AB magnitude system, from the HDF version 1 catalog; $I_{814,AB} = I_{814,ST} - 0.819$

[c]$U_{300,AB} - B_{450,AB}$ color. For those objects with $U_{300,AB} > 28.0$, close to the detection limit of the HDF for a 1″ source, a lower limit is given calculated for $U_{300,AB} = 28.0$.

[d]$B_{450,AB} - V_{606,AB}$ color.

[e]$B_{450,AB} - I_{814,AB}$ color.

[f]U- or B-band dropout (see text for details).

[g]Total exposure time (both red and blue gratings) in kiloseconds.

TABLE 2
CONFIRMED REDSHIFTS IN THE HDF

Name	z [a]	Q_z [b]	$r_{1/2}$ [c]		M_B [d]	SFR [e]	$W_0(\mathrm{Ly}\alpha)$ [f]	Ref [g]
			(″)	(h_{50}^{-1} kpc)		($h_{50}^{-2}\mathrm{M}_\odot$ yr^{-1})	(Å)	
hd4_1229_1791	0.483	3	0.53	4.15	-17.11	0.14[h]	$\cdots$	L4-515
hd2_2030_0287	2.267	4	0.36	4.37	-22.19	20.80	34.1	L2-14/M2-82.1/SC2-02
hd2_1410_0259	3.160	3	0.37	4.50	-22.16	14.36	6.2	L2-5?/C2P1/SC2-01
hd4_0367_0266	2.931	4	0.58	7.13	-22.66	17.36	$\cdots$	L4-3*
			(0.35, 0.44)	(4.29, 5.37)	(-22.55, -22.23)			
hd4_2030_0851	2.980	3	0.27	3.33	-22.34	14.52	$\cdots$	L4-200*/M4-363.0/SC4-04
hd3_0408_0684	3.233	4	0.21	2.53	-22.49	17.16	22.1	L3-120*
hd2_0698_1297	3.430	4	0.45	3.07	-22.85	23.76	14.5	L2-310*
			(0.22, 0.22)	(2.67, 2.72)	(-22.12, -21.99)			
hd2_0705_1366	3.368	4	0.14	1.75	-22.67	22.36	11.9	L2-331*/M2-637.0/SC2-11
hd2_1918_1912	star	$\cdots$	$\cdots$	$\cdots$	$\cdots$	$\cdots$	$\cdots$	L2-526/SC2-14
hd2_0434_1377	2.991	4	0.34	4.13	-22.83	20.72	$\cdots$	L2-334*/C2P2/M2-643.0/SC2-12
			(0.16, 0.17)	(1.95, 2.06)	(-22.15, -21.96)			
hd2_1359_1816	3.181	4	0.32	3.90	-22.99	24.92	$\cdots$	L2-495*
hd2_0624_1688	2.419	4	0.31	3.83	-21.60	6.56	9.3	L2-445/M2-824.0
			(0.26, 0.16)	(3.17, 1.96)	(-21.35, -20.40)			
hd2_0725_1818	2.233	4	0.26	3.21	-22.10	16.96	$\cdots$	L2-496/M2-903.0/SC2-12

[a]Redshift.

[b]Redshift quality. 3=redshift probable, with two or more spectral features identified; 4=redshift definite, with multiple spectral features identified.

[c]Half-light radius in arcsec measured from the "drizzled" images, and in kpc calculated assuming $H_0 = 50$ km s^{-1}Mpc^{-1}, $q_0 = 0.05$. Pairs of values in parentheses indicate subclumps for the preceding object. Values have not been corrected for the WFPC2 PSF FWHM$\sim 0\rlap{.}''14$; such a correction will make the median half-light radius 10% smaller, but will have a much larger effect on the smallest sources. For $q_0 = 0.5$, values would be ~ 0.6 times those listed here.

[d]Absolute B magnitude calculated from the observed $I814$ magnitude converted to Vega-based ($I_{814,Vega} = I_{814,ST} - 1.258$) and assuming $k-$corrections for a blue star-forming galaxy and $H_0 = 50$ km s^{-1}Mpc^{-1}, $q_0 = 0.05$. Pairs of values indicate subclumps for the preceding object, corrected by 0.1 mag (fainter) to account for the average additional flux in the *total* object we measure compared to the STScI HDF FOCAS catalog.

[e]Star formation rate calculated assuming $SFR = L_\lambda(1216)/1 \times 10^{40}\mathrm{M}_\odot$ yr^{-1} or $SFR = L_\lambda(1500)/1 \times 10^{40.1}\mathrm{M}_\odot$ yr^{-1}, for $H_0 = 50$ km s^{-1}Mpc^{-1}, $q_0 = 0.05$. For $H_0 = 100$ km s^{-1}Mpc^{-1}, $q_0 = 0.5$, values will be a factor of ~ 11 times lower.

[f]Rest equivalent width of Lyα emission line.

[g]Other published candidate lists in which object appears: C=Clements & Couch (1996); L=Lanzetta *et al.* (1996); M=Madau *et al.* (1996); S=Steidel *et al.* (1996b). For Lanzetta *et al.* a * indicates that the predicted redshift was $z > 2.2$.

[h]SFR derived from [O II] emission line, assuming $SFR = 2.4 \times 10^{-12} \times EW(O\ II) \times \exp(-0.4(M_B - \mathrm{M}_{\odot,B}))$ (Guzmán *et al.* 1996).

TABLE 3

Uncertain Redshifts in the HDF

Name	z [a]	Q_z [b]	$r_{1/2}$ [c] (″)	Ref [d]
hd4_0259_1947	3.30	2x	0.49	L4-553*
hd4_1076_1847	2.15	2	0.21	L4-544
hd4_0818_1037	2.04	2x	0.29	L4-252
hd2_1881_0374	2.58	2x	0.31	L2-42
hd4_1994_1406	3.63	1x	0.27	L4-371
hd4_1486_0880	2.47	2	0.36	L4-209
hd2_0853_0319	3.35	1x	0.68	L2-28
hd4_1341_0299	2.31	2x	0.25	L4-14/M4-85.2/SC4-01
hd2_1739_1258	2.72	2x	0.80	L2 -291
hd2_1410_1282	3.37	1x	0.30	L2-301
hd3_1455_0430	2.64	2	0.17	L3-38/SC3-01
hd2_0743_1844	2.39	1x	0.33	L2-501/C2P4

[a]Tentative redshift.

[b]Redshift quality. 1=SNR too low to discern features; 2=real features detected but redshift uncertain. An "x" indicates the redshift was derived from cross-correlating the spectrum with that of NGC 1741 (or, in the case of hd4_0818_1037, with that of the combined spectrum shown in Fig. 3).

[c]Half-light radius in arcsec measured from the "drizzled" images.

[d]Other published candidate lists in which object appears: C=Clements & Couch (1996); L=Lanzetta *et al.* (1996); M=Madau *et al.* (1996); S=Steidel *et al.* (1996b). For Lanzetta *et al.* a * indicates that the predicted redshift was $z > 2.2$.

Figure Captions

Figure 1. The DEEP sample of candidate high-redshift galaxies in the Hubble Deep Field. Only the 24 galaxies observed at Keck are shown. The images were excised from the version 1 "drizzled" HDF F450W, F606W, and F814W images, combined using the blue, green, and red color guns, respectively. The top twelve objects have confirmed redshifts, labeled in the upper right corner, and are presented in order of increasing redshift. The effect of redshift on the objects' apparent colors for $2 < z < 4$ is easily seen in this representation, with the lowest redshift galaxies appearing blue and the highest, green. The bottom twelve objects do not have confirmed redshifts, and are presented in order of increasing $B - V$ color. North is up, east is to the left, and each box is $10'' \times 10''$.

Figure 2. (a) One-dimensional optimally-extracted spectra of the twelve galaxies with confirmed redshifts, arranged in order of increasing redshift. Only the first galaxy has $z < 2.2$. Each spectrum has been smoothed by 11 pixels to reduce the noise. On the bottom of each panel of four spectra is the GHRS spectrum of the nearby irregular starburst galaxy NGC 1741 from Conti *et al.* (1996), redshifted for comparison with the HDF galaxies. The wavelengths of several rest-UV spectral features commonly seen in actively star-forming regions are indicated. In the spectrum of hd2_0698_1297, we have labeled the wavelengths of possible redshifted Si II $\lambda 1260$ and O I $\lambda 1303$ absorption at $z = 3.368$ from galaxy hd2_0705_1366, $4''$ away. **(b)** Two-dimensional spectra showing the region near Lyα for the six objects showing Lyα emission. Note the significant drop in continuum across the Lyα lines. Also shown are the [O II] $\lambda 3727$ emission line at $z = 0.483$ from hd_1229_1791 and the double Lyα emission line from object C4-09 of Steidel *et al.* (1996b). The small horizontal lines labeled a, b, and c indicate the spectra of hd2_0725_1818 ($z = 2.233$), hd2_0743_1844, and hd4_1076_1847 ($z \geq 1.01$), respectively. Each image section is 500 Å on the horizontal axis, with wavelengths increasing to the right; tick marks on the vertical axis are at $1''$ and $5''$ intervals.

Figure 3. Spectrum of hd4_1076_1847, the brightest galaxy in the sample. Despite the strong continuum and the presence of several absorption lines and a possible emission line (most of them more clearly visible in the two-dimensional spectrum), we are unable to determine a secure emission redshift. Two sets of Mg II absorption lines at $z = 0.879$ and 1.010 from galaxies $< 2''$ from the line of sight are indicated, and the absorption line tentatively identified as C IV at $z = 2.15$ (or Al II at $z = 1.93$) is labeled. Other absorption lines may be due to additional intervening systems at different redshifts.

Figure 4. Average spectrum of the 11 confirmed high-redshift galaxies in the HDF from the DEEP sample plus C4-09 of Steidel *et al.* (1996b). Note the weak Lyα emission line, the strong continuum break and broad absorption trough at Lyα, the weak emission lines

of He II and C III], and the absorption lines of Lyγ, Lyβ, Si II, O I, C II, Si IV, C IV, Fe II, and Al III. The high-ionization lines Si IV and C IV are weak and narrow compared to those seen in the spectra of high-metallicity hot stars (Walborn *et al.* 1996), implying that the average galaxy at $z \sim 3$ is not heavily metal-enriched.

Figure 5. Redshift vs. $I_{814,AB}$ for the confirmed sample. Also shown for comparison are the faint magnitude limit of the Canada France Redshift Survey (Lilly *et al.* 1996); three lines corresponding to unevolved L*, 10 L*, and 100 L* blue star-forming galaxies; the five confirmed high-redshift objects in the HDF observed by Steidel *et al.* (1996b; × symbol); two galaxies that have been interpreted as possible primeval galaxies, IRAS 10214+4724 (Rowan-Robinson *et al.* 1991) and CNOC cB58 (Yee *et al.* 1996), and the gravitationally lensed high-redshift galaxies discovered by Trager *et al.* (1996; open circles), although all four of those galaxies may be gravitationally lensed and thus magnified by up to a factor of 10; a Lyα- and Hα-emitting galaxy at $z = 2.5$ found near a QSO absorption-line cloud (Malkan *et al.* 1995; open box symbol); and two objects at $2 < z < 3$ in the Flanking Fields that were selected based on their compact morphology and high surface brightness ("serendipitous"; see Phillips *et al.* 1996 for more details). The present sample probes significantly fainter than most previous studies of high-redshift galaxies: the confirmed sample comprises objects that are barely more luminous than L* galaxies today.

Figure 6. Color-color distributions of galaxies in the HDF. **(a)** $B_{450,AB} - I_{814,AB}$ vs. $U_{300,AB} - B_{450,AB}$. **(b)** $V_{606,AB} - I_{814,AB}$ vs. $B_{450,AB} - V_{606,AB}$. The 11 confirmed high-redshift galaxies are indicated by open hexagons, the 12 galaxies with unconfirmed redshifts are indicated by open circles, the Galactic star is indicated by a star symbol, the galaxy at $z = 0.483$ is indicated by an open triangle, and additional galaxies from the HDF WF2 catalog that we did not observe are shown by open squares, to indicate the field galaxy population. (Note that we have omitted field galaxies from the WF3 and WF4 chips for clarity; the actual density of field galaxies compared to the observed sample is thus about three times higher than shown.) Candidate galaxies with $U_{300,AB} \geq 28.0$ are shown at a conservative lower limit corresponding to $U_{300,AB} = 28.0$ and are indicated by a vertical line. Also shown (× symbol) are the five confirmed high-redshift galaxies of Steidel *et al.* (1996b). The solid lines indicate the regions of color-color space we used to select our U-band (*a*) and B-band (*b*) dropout candidates. The regions chosen by Madau *et al.* (1996) to select high-redshift candidates are indicated by dotted lines. There are five objects that do not satisfy those criteria, even after including the higher lower limits of Madau *et al.*, and yet are confirmed to have $z > 2.9$.

Figure 7. Rest-frame B absolute magnitude (M_B) vs. logarithm of half-light radius ($r_{1/2}$) in kpc for our confirmed sample of high redshift galaxies (open hexagons, large for

total objects and small for subclumps) as well as for a representative sample of various types of local galaxies: ellipticals, dwarf ellipticals/spheroidals, and spiral bulges (Bender *et al.* 1992); spirals (total galaxy) and irregulars (de Vaucouleurs *et al.* 1991); H II galaxies (Telles 1995); and Compact Narrow Emission Line Galaxies (CNELGs; Koo *et al.* 1994). Despite their high luminosities (i.e. $\sim$1-2 magnitudes above L_*), high redshift galaxies have very small total sizes ranging from $1.7 < r_{1/2} < 7 \ h_{50}^{-1}$ kpc (for $q_0 = 0.05$) with a median value $r_{1/2} = 3.6 h_{50}^{-1}$ kpc. For $q_0 = 0.5$, values would be ~ 0.6 times those shown here. Radii have not been corrected for the WFPC2 PSF FWHM$\sim 0''\!.14$; such a correction will make the median half-light radius 10% smaller, but will have a much larger effect on the smallest sources. This places them at the bright end of the sequence defined by local HII galaxies, somewhat smaller than average massive galaxies today but consistent with the sizes of spiral bulges.
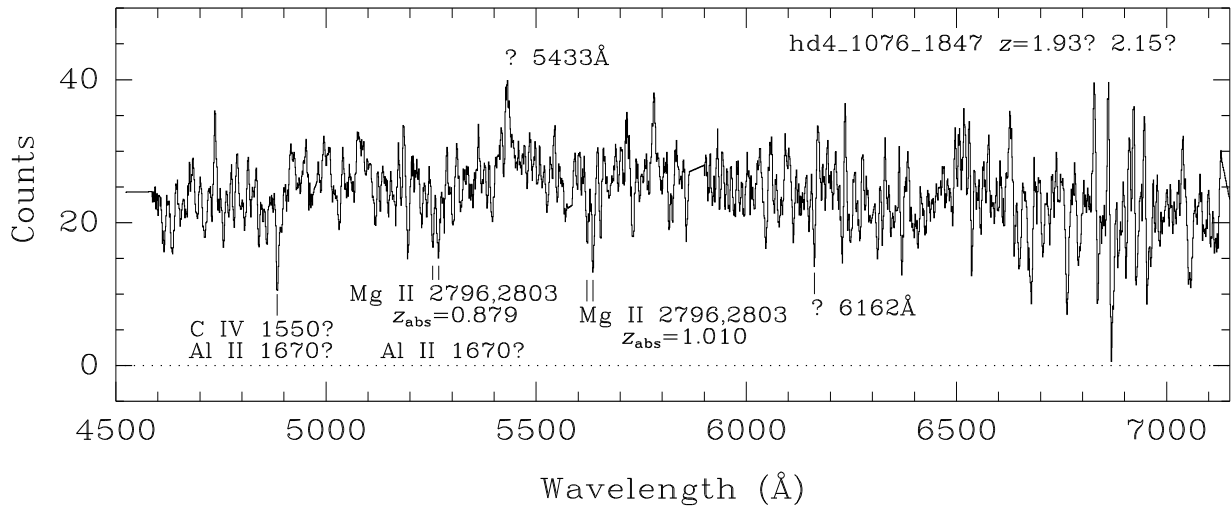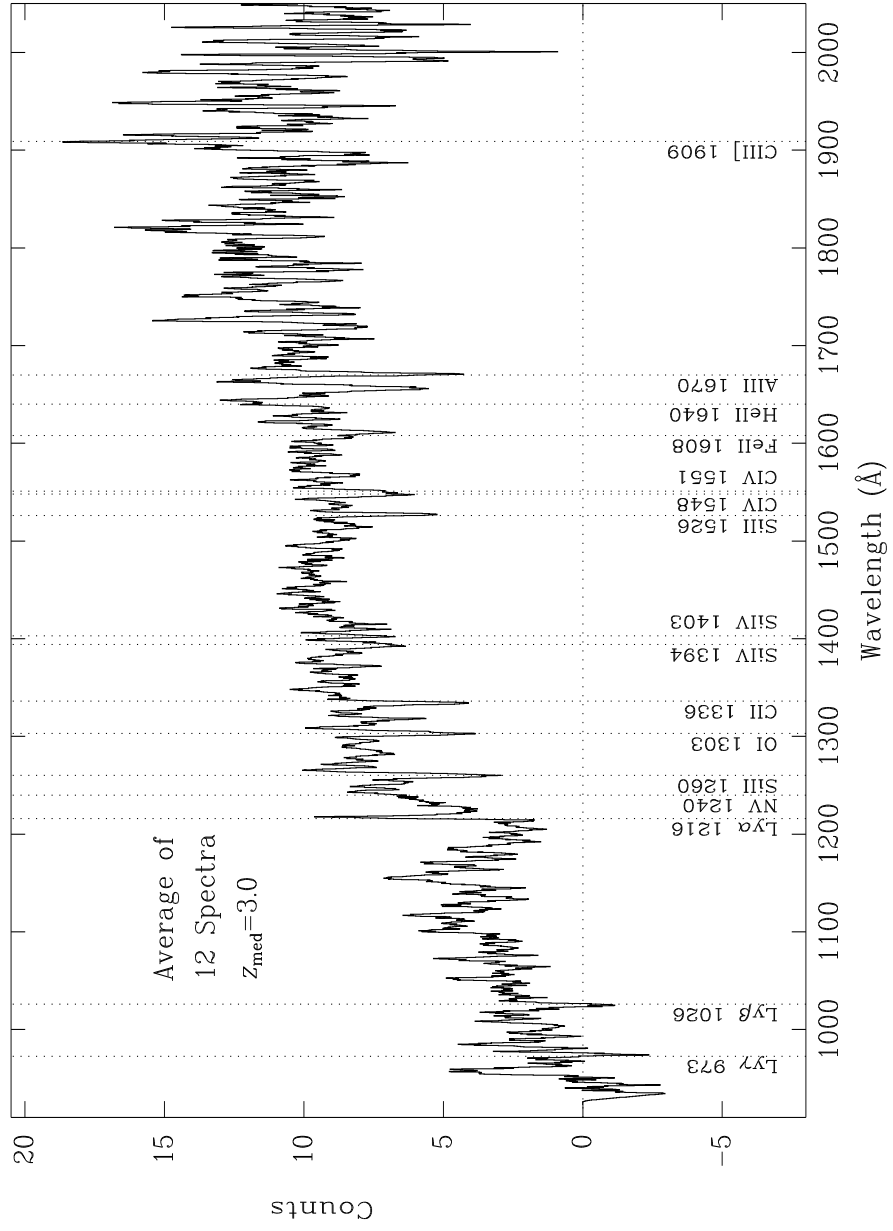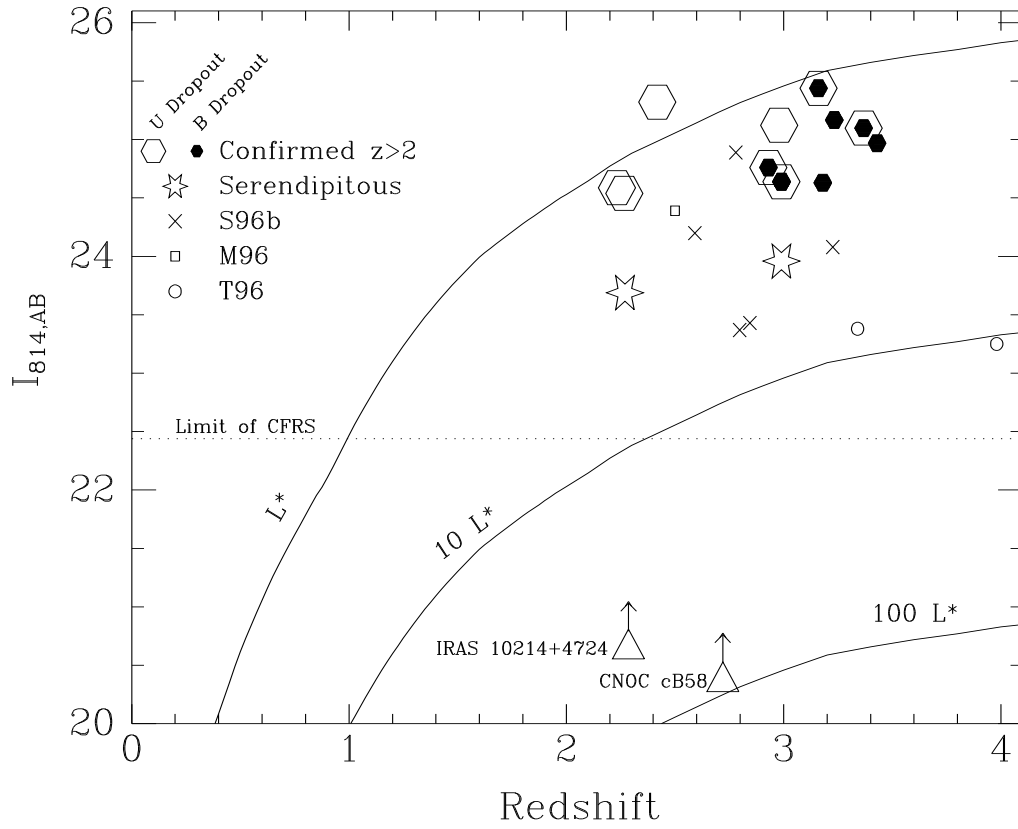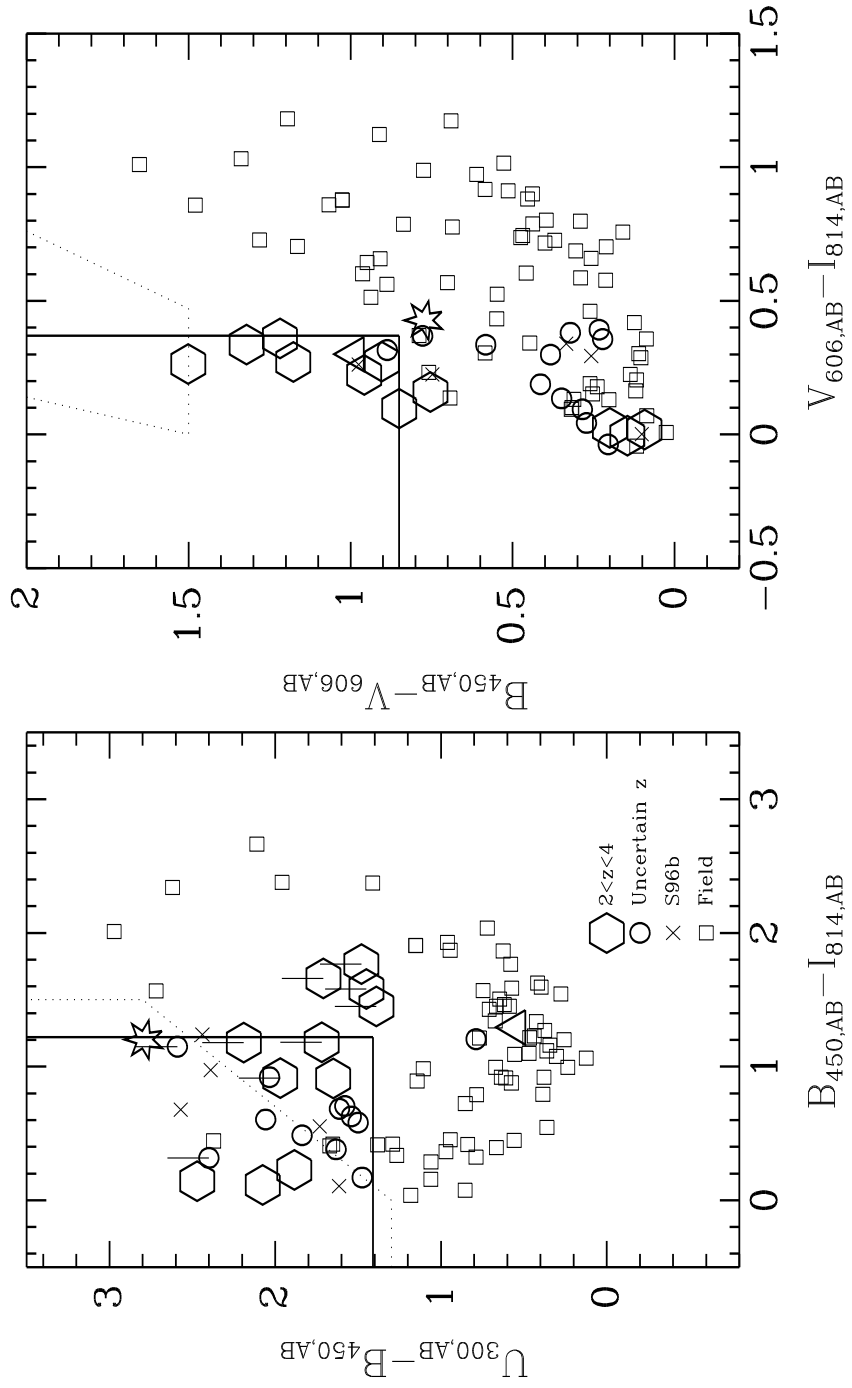
Fig. 3

Fig. 4

Fig. 5

Fig. 6
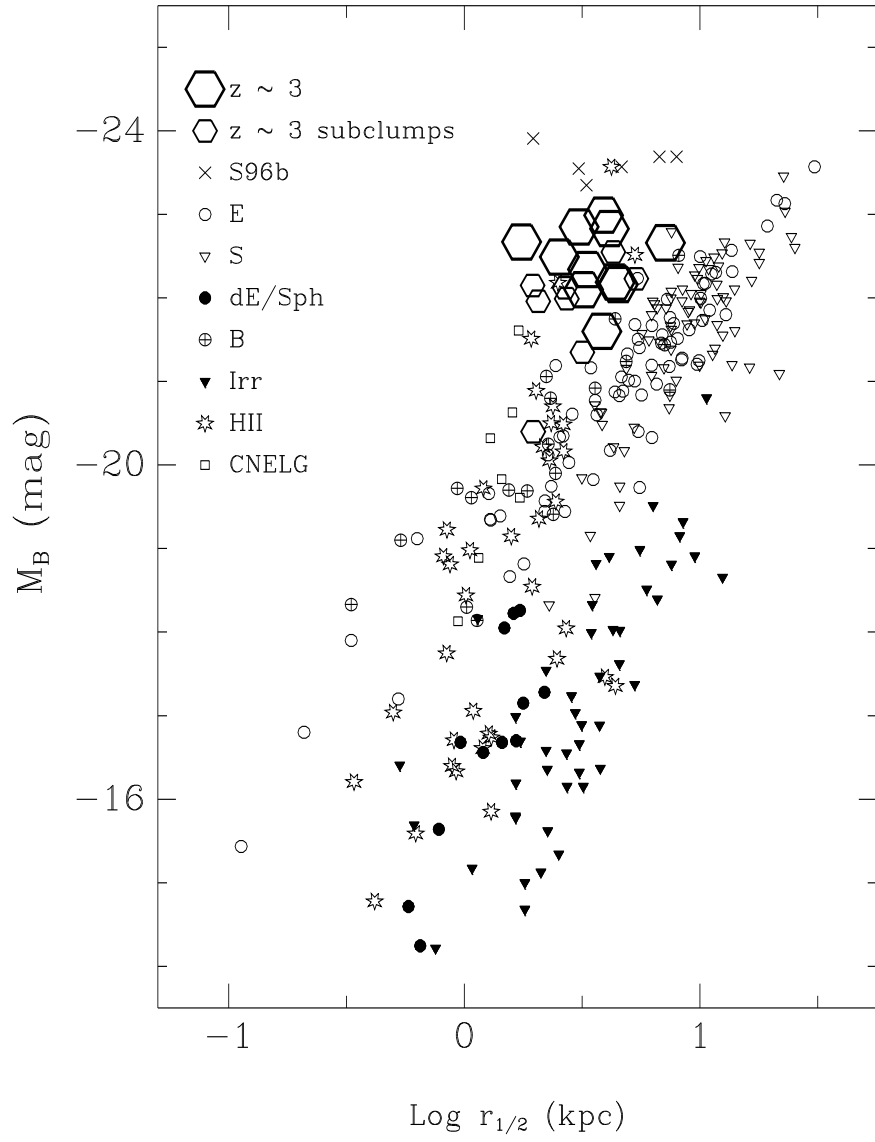
Fig. 7

This figure "fig1.jpg" is available in "jpg" format from:

http://arxiv.org/ps/astro-ph/9612239v1

This figure "fig2a1.gif" is available in "gif" format from:

http://arxiv.org/ps/astro-ph/9612239v1

This figure "fig2a2.gif" is available in "gif" format from:

http://arxiv.org/ps/astro-ph/9612239v1

This figure "fig2b.jpg" is available in "jpg" format from:

http://arxiv.org/ps/astro-ph/9612239v1

This figure "fig2a3.gif" is available in "gif" format from:

http://arxiv.org/ps/astro-ph/9612239v1